J Mater Sci (2010) 45:5660–5668
DOI 10.1007/s10853-010-4631-0

Meso-macroporous monolithic $CuO–CeO_2/\gamma$-Al_2O_3 catalysts and their catalytic performance for preferential oxidation of CO

Chunlei Gu · Jie Miao · Yuan Liu · Yaquan Wang

Received: 19 December 2009 / Accepted: 17 May 2010 / Published online: 3 June 2010

Abstract Meso-macroporous monolithic $CuO–CeO_2/\gamma$-Al_2O_3 catalysts were prepared and tested for preferential oxidation of carbon monoxide in hydrogen-rich gases. The catalysts were characterized with photographs, SEM, N_2 adsorption–desorption, XRD, HRTEM, and TPR techniques. $CuO–CeO_2$ catalysts were evenly coated onto the walls of γ-Al_2O_3 monolith macropores with ceria and copper oxide highly dispersed. The prepared meso-macroporous monolithic $CuO–CeO_2/\gamma$-Al_2O_3 catalysts can remove CO from H_2-rich gases to ppm level at high space velocity, indicating that they are a kind of promising structured catalyst.

Introduction

Hierarchically porous materials with multiple-scale porous structure, generally micro-meso-macroporous or meso-macroporous structure, have attracted great attention recently due to their potential applications in various fields, such as heterogeneous catalysts [1], chemical separations [2], electrode materials [3], etc.

The sizes of the macropores and the mesopores are generally in the range of tens of microns and several nanometers, respectively, in the meso-macroporous materials. As catalysts or catalyst supports, the macropores favor the mass transfer and the mesopores can provide with high surface area, so this kind materials are of great potential in the catalysis area. For example, macroporous materials as catalysts or catalyst supports applied to large molecule reactions exhibit very good catalytic performance [1]. Meso-macroporous silica, titania, zirconia, carbon, and molecular sieves [4–12] have been prepared and exhibit good catalytic performance for some reactions, such as photo catalysis [13], epoxidation of cyclohexene [14], Friedel–Crafts alkylation [15], and total oxidation of toluene [9]. Some materials, such as silica, titania, zirconia, carbon, and polymer, have been made to monolithic shape with hierarchically pores [16–19]. Studies on the catalytic performance of meso-macroporous materials (not monolith) can be found as listed above, while studies on monolithic macroporous catalysts and their catalytic performance can hardly be found till now.

In recent years, the proton exchange membrane fuel cell (PEMFC) has been attracting great attentions both for its stationary and portable applications [20]. In particular, the PEMFC has been considered as a power generator for compact devices, such as laptops, mobile phones, and MP3 players, due to its advantages of easy scale-down, high-power density, and mild operating temperature [21]. Pure hydrogen is the fuel for PEMFC. The hydrogen productions via steam reforming or partial oxidation of hydrocarbons followed by water gas shift reaction are well developed and widely used in industry [22]. However, the systems are too huge to be fit for the compact PEMFC applications. Thus, to develop the compact and mobile hydrogen production system is a crucial challenge for practical application of fuel cells.

The hydrogen-rich gases come from methanol reforming, a potential route for small scale hydrogen production,

C. Gu · J. Miao · Y. Liu (✉)
Tianjin Key Laboratory of Applied Catalysis Science and Engineering, Department of Catalysis Science and Technology, School of Chemical Engineering and Technology, Tianjin University, Tianjin 300072, People's Republic of China
e-mail: yuanliu@tju.edu.cn; rispringsun@yahoo.cn

Y. Wang
Key Laboratory for Green Chemical Technology of Ministry of Education, School of Chemical Engineering and Technology, Tianjin University, Tianjin 300072, People's Republic of China

or other hydrocarbon reforming combined with water gas shift reaction generally contain 0.5–2.0% of CO [23], while PEMFC electrodes are extremely sensitive to even trace amount of carbon monoxide of 10–100 ppm [24]. As a consequence, the hydrogen fed to the anode should be purified to almost free of CO. Among the methods available for removing carbon monoxide from hydrogen-rich stream, preferential oxidation (PROX) seems to be the simplest and most effective one.

So far, extensive studies have been done to reduce the volume of reactors by increasing the intrinsic activity of the catalysts. Two categories of catalysts have been proposed in literatures for CO-PROX reaction. One is the noble metal-based catalysts [25, 26]. The other is the transition metal oxide catalysts, in which $CuO–CeO_2$ [27–29] and $Co_3O_4–CeO_2$ [30, 31] are studied extensively. Especially, $CuO–CeO_2$ exhibits high selectivity and activity for CO-PROX in hydrogen-rich gases, and is a promising candidate.

As for the reactor configurations, monolithic catalysts and micro-channel reactors have been proposed as the effective ways for the miniaturization [32–34]. Monolithic reactors with channel size in millimeter scale can be operated at higher space velocity than the conventional particle packed bed reactors, and can reduce the reactor volume to some extent [33]. Micro-channel reactor with channel diameters in the order of 100–500 μm can reduce the reactor size more effectively [34]. However, the volume of the reactors is still too large and CO cannot be purified to ppm level at high space velocity [35, 36].

In our previous work, a simple method for preparing meso-macroporous monolithic Al_2O_3 have been developed [37], and it was found that meso-macroporous monolithic Al_2O_3 supported Pt–K catalysts showed good catalytic performance for CO-PROX [1]. As stated above, $CuO–CeO_2$ is an important and potential catalyst for CO-PROX. Thus, in this work, meso-macroporous monolithic γ-Al_2O_3 supported $CuO–CeO_2$ catalysts were prepared and their catalytic performance for CO-PROX reaction was investigated.

Experimental

Preparation of meso-macroporous monolithic $CuO–CeO_2/\gamma$-Al_2O_3 catalysts

Preparation of monolithic polystyrene (PS) foam template

The polystyrene foams were obtained by polymerization of styrene in reverse concentrated water-in-oil (W/O) emulsions, as reported in our previous paper [37]. In brief, the monomer styrene, the cross linking agent divinyl benzene (DVB), azodiisobutyronitrile (AIBN), and Span 80 were introduced into a flask to form a homogeneous phase. Then deionized water was added into the homogeneous phase to obtain reverse concentrated water-in oil (W/O) emulsion, which was put into sealed glass molds for the styrene polymerization. The resultant polystyrene monoliths were removed from the molds, washed with deionized water, and ethanol to remove surfactant species, dried at 60 °C for 24 h. Thus, the polystyrene monolithic templates were obtained.

Preparation of meso-macroporous alumina monolith

Meso-macroporous alumina monoliths were prepared by impregnating macroporous monolithic polystyrene foams with alumina sols, as reported in literature [37]. The alumina sol was impregnated into the polystyrene template pores under modest vacuum, and the coated templates were dried at 60 °C for 12 h. The coating and drying procedures were repeated for several times. Then, the coated templates were calcined in air at 600 °C for 4 h to obtain meso-macroporous alumina monoliths.

Preparation of meso-macroporous monolithic $CuO–CeO_2/\gamma$-Al_2O_3 catalysts

Meso-macroporous monolithic $CuO–CeO_2/\gamma$-Al_2O_3 catalysts, denoted as $CuO–CeO_2/M$-γ-Al_2O_3, were prepared by co-impregnating the alumina monoliths with a mixed aqueous solution of $Ce(NO_3)_3$ and $Cu(NO_3)_2$ for 24 h. After the impregnation, the samples were dried at 80 °C for 24 h and then calcined at 600 °C for 3 h in air. The total content of $CuO–CeO_2$ in the monolith catalysts is 35% in weight. The molar ratio of n_{Cu}:($n_{Cu} + n_{Ce}$) in the catalysts is 0.25.

Characterization

Photographs of the monoliths were taken by using an Olympus 17000 digital camera.

Scanning electron microscopy (SEM) tests were performed on a Philips XL-30ESEM microscope with Au-sputtered specimen to observe the macroporous structures of the samples.

Nitrogen adsorption and desorption isotherms were determined on a Micromeritics apparatus of model ASAP-2020 at −196 °C. The specific surface areas were calculated by the BET method and the pore size distributions were calculated based on the desorption branch of the isotherm by BJH model.

Powder X-ray diffraction (XRD) patterns of the samples were recorded on Rigaku D/max 2500v/pc X-ray diffractometer in order to identify the different phases present in the samples and to determine their crystalloid. Copper Ka

radiation ($\lambda = 0.15406$ nm) was used with a power setting of 40 kV and 200 mA (Scan rate = 5° min^{-1}).

High-resolution transmission electron microscopy (HRTEM) pictures were obtained on a Technai G2 F20 microscope operated at 200 kV. Samples were finely grounded in a mortar to fine particles and dispersed ultrasonically in ethanol. The well-dispersed samples were deposited on a grid covered by a porous carbon film for measurements. The energy-dispersive X-ray spectroscopy (EDX) analysis was performed along with observation of TEM. The probe resolution of EDX is 1 nm and the species within 5 nm circle have some effect on the results of measurement.

Temperature programmed reduction (TPR) analysis was made on a conventional equipment with a thermal conductivity detector (TCD) at a 5% H_2/Ar mixture flow of 30 cm^3 min^{-1} and a heating rate of 10 °C min^{-1}. 50 mg samples were used.

Catalytic performance test

Catalytic performance tests were carried out in a fixed bed tubular reactor operated at atmospheric pressure. In each run, a piece of monolith was put into a thermal resistant silica tube, and the silica tube was connected with two quartz tubes at its both ends. The reaction temperature was monitored by a K-type thermocouple placed in the monolithic catalysts and controlled by a temperature controller. The reaction mixtures consisted of 1 vol.% CO, 1 vol.% O_2, and 50 vol.% H_2 in N_2. The mass space velocity was 20,000 mL g_{cat}^{-1} h^{-1}, corresponding to volume space velocity of 16,000 h^{-1}. In the case of simulated reformat (1 vol.% CO, 1 vol.% O_2, 50 vol.% H_2, 15 vol.% CO_2, 8 vol.% H_2O in N_2), the mass space velocity was 15,000 mL g_{cat}^{-1} h^{-1}, corresponding to the volume space velocity of 12,000 h^{-1}. The product mixtures were analyzed with a SP-3420 gas chromatograph (GC) equipped with a TCD and a column packed with 5A molecular sieve. A methane convertor was used to magnify the CO signals. A hydrogen flame ionization detector (FID) was equipped to detect the CH_4 and CO signals. The detection limit for CO is about 5 ppm. CO conversion and the selectivity of O_2 to CO oxidation were calculated by the following equations:

$$\text{Conversion of CO } (\%) : X_{CO} = \frac{[CO]_{in} - [CO]_{out}}{[CO]_{in}} \times 100, \quad (1)$$

$$\text{Selectivity of } CO_2(\%) : S_{CO_2} = \frac{[CO]_{in} - [CO]_{out}}{2 \times \left([O_2]_{in} - [O_2]_{out}\right)} \times 100. \quad (2)$$

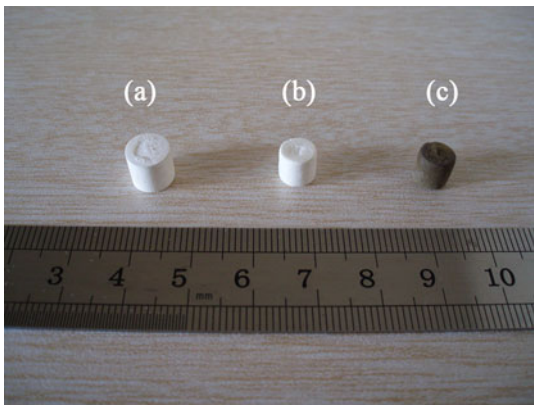

Fig. 1 Photographs of **a** PS template, **b** M-γ-Al_2O_3 support, **c** CuO–CeO_2/M-γ-Al_2O_3

Results and discussion

Catalyst characterization

Photographs and SEM images

Figure 1a shows a representative optical photograph of the prepared PS monolith with the cylindrical shape, and Fig. 1b and c are the corresponding macroporous alumina monolith and monolithic catalyst. During the calcination to remove the organic templates, shrinkage of the monoliths happened. Comparing to the original PS foams, the alumina and catalyst monoliths replicated the bulk shape of the templates with the shrinkage of approximately 30% in bulk dimensions. The monolithic catalysts, as shown in Fig. 1c, take on a dim-gray color, which is due to the loading of CuO–CeO_2.

The PS monoliths can be made to any shape wanted just by cutting them with a knife; consequently the monolithic catalysts can be made to any shape too. So their utilization is convenient and flexible.

Figure 2a is the representative SEM pictures of the polystyrene foam monoliths, in which the macropores are in spherical shape with the diameter in the range of 10–40 μm. The spherical macropores are interconnected via windows with the diameters approximately of 1–20 μm. The microscopic appearance of the macroporous alumina monolith (Fig. 2b) is the replica of the polystyrene foam with the shrinkage taken into account. The wall thickness of the alumina support is about 1–2 μm (Fig. 2c, e). Loading of CuO–CeO_2 does not change the macroporous structure of the monoliths (Fig. 2d). As can be seen from Fig. 2f, the CuO–CeO_2 was evenly coated on the walls of the macropores.

The size of the macropores is adjustable by controlling or changing the preparation conditions, such as the ratio of water to oil phase, calcination temperature, etc. [37].

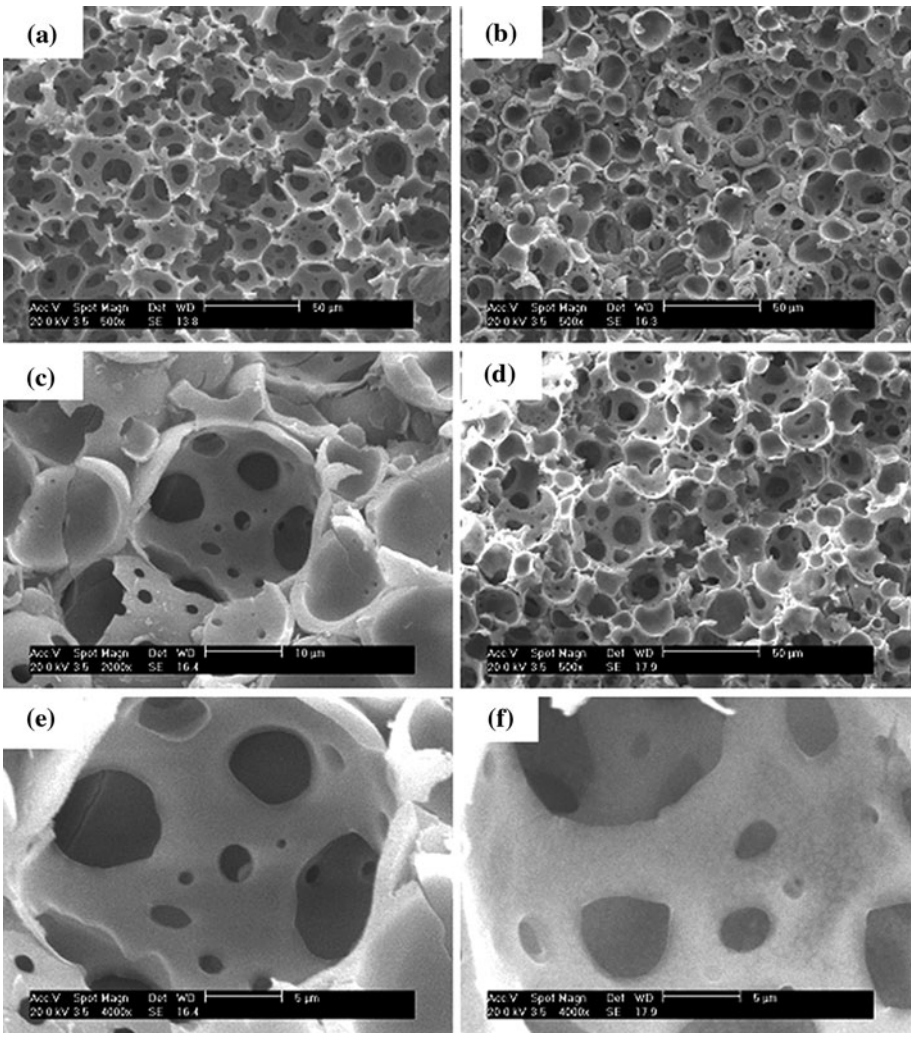

Fig. 2 SEM images of **a** PS; **b**, **c**, **e** M-γ-Al_2O_3; **d**, **f** CuO–CeO_2/M-γ-Al_2O_3. *Scale bar*: **a**, **b**, **d** 50 μm; **c** 10 μm; **e**, **f** 5 μm

N_2 adsorption–desorption

Table 1 lists the BET surface areas, S_{BET}, and the average pore diameters of the samples. Both the monolithic support and the catalysts have large specific surface areas, and the S_{BET} of the alumina monolith is obviously higher than that of CuO–CeO_2/alumina monolith. Figure 3a indicates that both of the samples present the IV(b) type isothermal curve characters and II type isothermal curve characters with the hysteretic loops showing the existence of mesopores in the monoliths. However, the hysteretic loop types of these two samples are different. The hysteretic loop of the support belongs to "ink bottle" type, whereas that of the catalyst is "slot" type. Loading of CuO–CeO_2 resulted in a decrease of the specific pore volume, pore diameter (Table 1), and the amount of nitrogen adsorbed (Fig. 3). The change of the pore structure resulted from the loading should be due to the blocking of the micropores and mesopores of the support by CuO–CeO_2 particles.

Table 1 BET specific surface area, BJH pore diameter, and volume of the monolith support and catalyst

Sample	BET surface area (m^2 g^{-1})	Pore diameter (nm)[a]	Pore volume (cm^3 g^{-1})
M-γ-Al_2O_3	249	4.4	0.332
CuO–CeO_2/M-γ-Al_2O_3	149	4.3	0.220

[a] BJH desorption pore diameter

The N_2 adsorption–desorption results of Fig. 3 and Table 1 indicate that the prepared monoliths are mesoporous with the mesopore sizes centered at about 4.4 nm. Thus, the SEM and N_2 adsorption–desorption results clearly show that the obtained alumina monoliths and the CuO–CeO_2/alumina monoliths are of hierarchically porous, namely meso-macroporous structure.

Powder X-ray diffraction (XRD)

Figure 4 presents the XRD patterns of the alumina monolithic supports and the catalysts. It is indicated that the

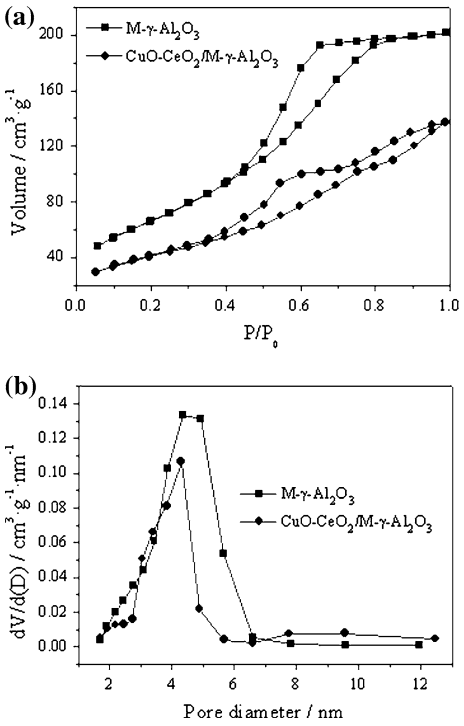

Fig. 3 **a** N_2 adsorption–desorption isotherms and **b** BJH pore diameter distribution curves of the support and catalyst

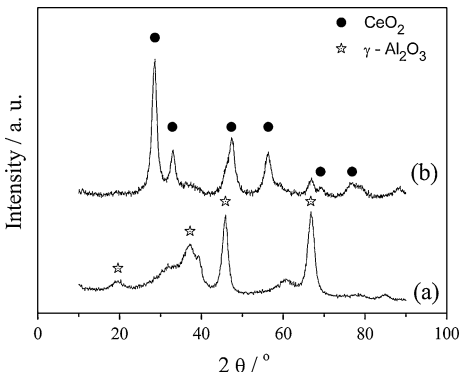

Fig. 4 XRD patterns of **a** M-γ-Al_2O_3 and **b** CuO–CeO_2/M-γ-Al_2O_3

alumina monolith is of γ-Al_2O_3 phase. Loading of CuO–CeO_2 leads to the appearance of obvious ceria diffraction peaks in its typical fluorite structure. The mean diameter of the ceria crystallites, calculated from the X-ray line broadening according to the Scherrer equation, is about 7.9 nm. No diffraction peaks related to Cu-containing phases can be detected in the XRD patterns, suggesting that the copper oxide is highly dispersed. The average mesopore size of the alumina supports is 4.4 nm, and the average crystallite size of ceria is 7.9 nm. Therefore, the ceria particles are not in the mesopores of the support. However, the mesopores and the high surface area of the alumina support are beneficial for the high dispersion of ceria and copper oxide precursors in the impregnation process, leading to the high dispersion of CeO_2 and CuO on the macropore walls of alumina.

High-resolution transmission electron microscopy

A typical HRTEM micrograph of CuO–CeO_2/M-γ-Al_2O_3 is shown in Fig. 5a, b, c. The crystalline lattice fringes of ceria (111) can be clearly seen from Fig. 5. The crystal sizes of ceria are about 8 nm in accordance with the size derived from XRD results.

The EDX analysis results of the three regions of A, B and C are presented in Fig. 5a′, b′, and c′. Some elements in small quantity are present in the EDX results, which should be due to the interference of the elements near the spots. In Fig. 5a′, copper and cerium are the dominate elements and aluminum elements are neglectable. This indicates that the "A" region in Fig. 5a presents the area of copper species dispersed on ceria. In Fig. 5b′, all of copper, cerium, and aluminum were detected, which shows an example area of both ceria and alumina supported copper. In Fig. 5c′, both copper and aluminum element are present and nearly no cerium can be detected in the EDX results, so this is the area of copper species dispersed on alumina. Therefore, as the EDX analysis results show, the highly dispersed copper oxide species exist in three categories, the first is dispersed on ceria oxide (as illustrated at A in Fig. 5a), the second is on γ-alumina surface with parts of copper oxide particles' fringe in contact with ceria (B in Fig. 5b), and the third is on γ-alumina surface (C in Fig. 5c) with no interaction to ceria.

Temperature programmed reduction (TPR)

H_2 TPR profiles of CuO–CeO_2/M-γ-Al_2O_3 monoliths are shown in Fig. 6. For comparison, the profiles of CeO_2/M-γ-Al_2O_3 and CuO/M-γ-Al_2O_3 are also included.

The TPR profile of CeO_2/M-γ-Al_2O_3 shows two peaks at about 490 and 800 °C, attributed to the reduction of the surface and the bulk ceria, respectively. The reduction temperatures are lower, but the hydrogen consumptions are higher, than that of the pure ceria, which should be due to the high dispersion and the interaction of ceria with alumina [38]. For CuO/M-γ-Al_2O_3, the only reduction peak at about 216 °C is attributed to the reduction of Cu^{2+} in copper oxide on alumina to Cu^0.

The TPR profile of CuO–CeO_2/M-γ-Al_2O_3 catalysts exhibits three reduction peaks centered at 132, 157, and 202 °C. Compared with CuO/M-γ-Al_2O_3, the peak at 202 °C, denoted as β, is assigned to the reduction of CuO supported on alumina. The other two, denoted as α_1 and α_2 are the reduction of highly dispersed copper oxide in interaction with ceria, specifically corresponding to copper

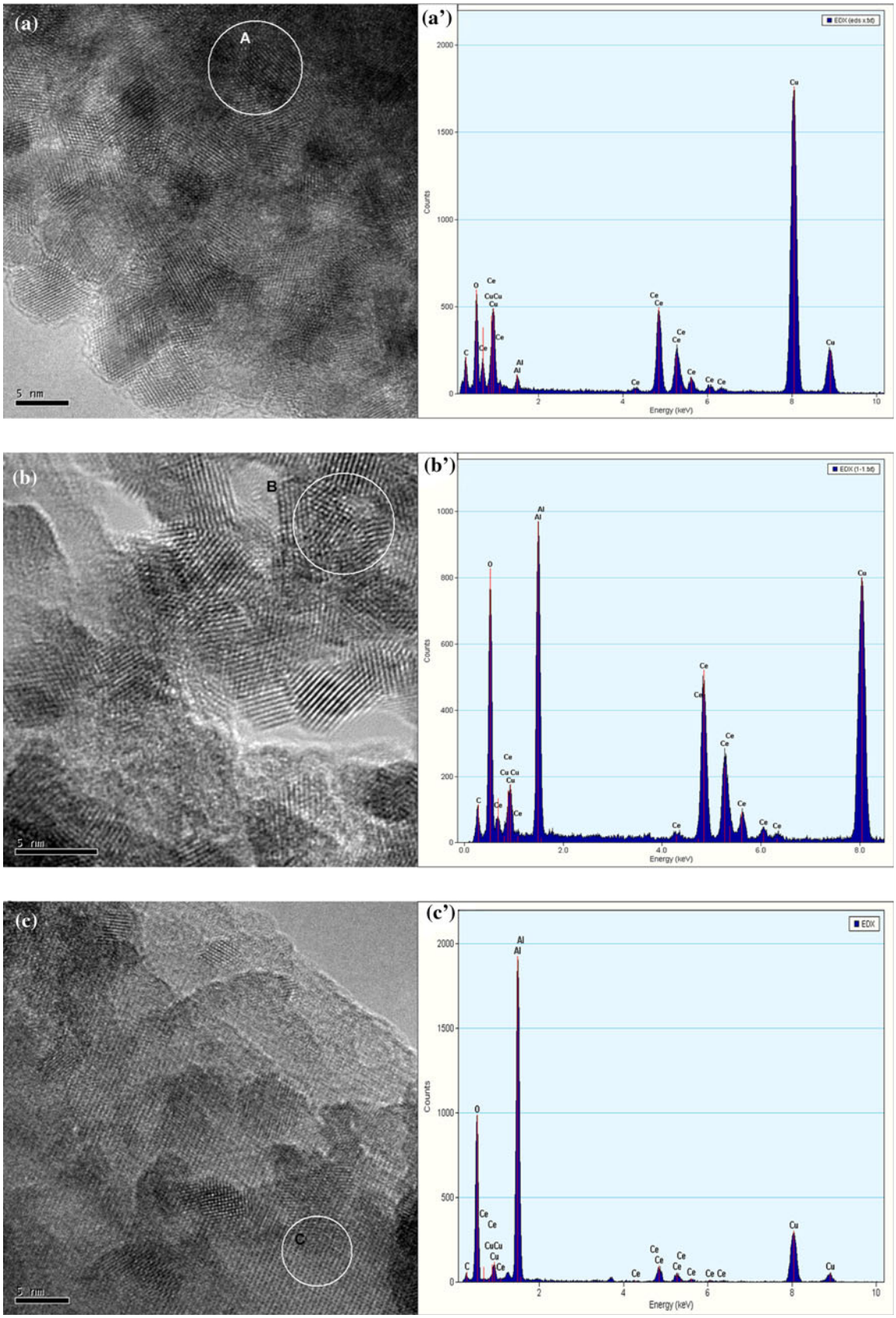

Fig. 5 TEM images of $CuO–CeO_2/M\text{-}\gamma\text{-}Al_2O_3$ and EDX results

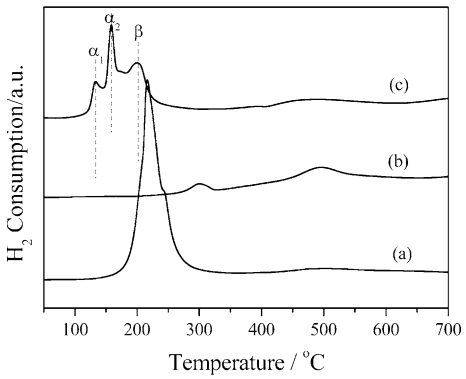

Fig. 6 TPR profiles of **a** CuO/M-γ-Al_2O_3; **b** CeO_2/M-γ-Al_2O_3; **c** CuO–CeO_2/M-γ-Al_2O_3

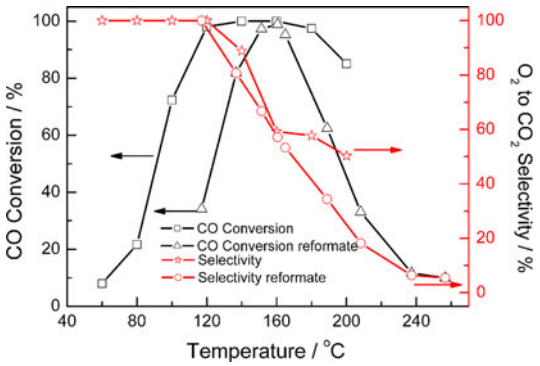

Fig. 7 The variation of CO conversion and O_2 selectivity to CO oxidation with reaction temperature over CuO–CeO_2/M-γ-Al_2O_3 monolith with Cu/(Ce + Cu) molar ratio of 0.25.(□, ☆: CO conversion, selectivity in 1 vol.% CO, 1 vol.% O_2, 50 vol.% H_2 in N_2, at GHSV = 16,000 h^{-1}; Δ, ○: CO conversion, selectivity in 1 vol.% CO, 1 vol.% O_2, 50 vol.% H_2, 15 vol.% CO_2, 8 vol.% H_2O in N_2 at GHSV = 12,000 h^{-1})

oxide supported on ceria as illustrated in Fig. 5—A, and the copper oxide supported on alumina and in interaction with ceria as shown in Fig. 5—B, respectively.

The ceria-supported copper oxide species are reduced at lower temperatures, compared with copper supported on alumina. It has been reported that ceria promotes the reduction of highly dispersed copper oxide species. Jiang et al. [39] observed a shift of copper oxide reduction peak from 310 to 250 °C as adding CeO_2 into CuO/Al_2O_3. Many studies on the reduction behavior of CeO_2 supported highly dispersed CuO are carried out, and two kinds of viewpoints have been proposed. Generally CeO_2 supported highly dispersed CuO exhibits two reduction peaks below 200 °C due to the copper oxide reduction. One of the viewpoints suggests that both of the peaks are attributed to the reduction of the highly dispersed copper oxide, but at different dispersion states [40]. The other points out that the two peaks correspond to the successive reduction of Cu^{2+} to Cu^{1+} and then Cu^{1+} to metal copper [41].

What is the detailed reduction process is not the focus of this article. However, both of the viewpoints suggested that the reduction peaks below 200 °C are attributed to the highly dispersed copper oxide on ceria, which are in interaction with ceria. This kind of copper contributes to the high activity of CuO–CeO_2 for CO oxidation [42]. Copper oxide supported on ceria is very active for CO oxidation, while copper oxide supported on alumina is much less active [43]. Therefore, here, the reduction peaks α_1 and α_2 are attributed to the reduction of the highly dispersed copper oxides interacted with ceria, which are the active components for the CO-PROX.

Catalytic performance

The catalytic performance of the CuO–CeO_2/M-γ-Al_2O_3 monolith for CO-PROX in hydrogen-rich gas is shown in Fig. 7. The prepared CuO–CeO_2/M-γ-Al_2O_3 monoliths are much active and selective for CO-PROX. Especially, over CuO–CeO_2/M-γ-Al_2O_3 with Cu/(Ce + Cu) molar ratio of 0.25, CO conversion of nearly 100% can be obtained in the temperature range of 120 to 180 °C (see Fig. 7). The high activity can be attributed to the high dispersion of copper oxide and the interaction of copper with ceria. The active sites located at the interfaces between copper oxide and ceria, which has been clarified by Gamarra et al. [44]. The catalyst shows 100% selectivity for O_2 to CO oxidation below reaction temperature of 120 °C (Fig. 7) and the selectivities are higher than 50% in the temperature range of 120 to 180 °C. The catalytic performance in the simulated reformate gas mixture of 1 vol.% CO, 1 vol.% O_2, 50 vol.% H_2, 15 vol.% CO_2, 8 vol.% H_2O in N_2 was investigated at space velocity of 12,000 h^{-1}. The maximum CO conversion of 99% was achieved at 170 °C.

As to the CO-PROX catalysts for hydrogen generators, some excellent work has been reported recently as listed in Table 2. Papavasiliou et al. [45] coated a CuO–CeO_2 on aluminum metal foam, at volume space velocity of 4,718 h^{-1}; CO in hydrogen-rich gases can be removed to ppm level. Maeda et al. [46] and Galletti et al. [47] studied a 4 wt% Pt–0.5 wt% Fe/mordenite ceramic monolith and a 1% Pt/3A zeolite–γ-Al_2O_3 micro-channel catalyst for CO-PROX in H_2-rich gases, and found that CO can be purified to ppm level at volume space velocity of 9,500 and 4,800 h^{-1}, respectively. With the comparable reactant composition, over the macroporous monolithic CuO–CeO_2/M-γ-Al_2O_3 catalysts prepared in this work, CO can be purified to ppm level at the volume space velocity of 16,000 h^{-1}, which is much higher than those over the metal foam and the micro-channel reactor reported in the above literatures. As stated in the above introduction section, the compact PROX reactor is of great significance. In the CO removal process, higher volume space velocity

Table 2 Comparison of catalyst performance of this work with that reported in the literatures

The composition of the monoliths	Composition of reactant	GHSV (h^{-1})	Maximum conversion (%)	Temperature (°C)	References
Cu/(Cu + Ce) = 0.25 net mass of CuO–CeO_2 is 45 mg	1% CO 1% O_2 50% H_2 in N_2, $\lambda = 2$	16,000	>99	120–180	This work
	1% CO 1% O_2 50% H_2 15% CO_2 8% H_2O in N_2, $\lambda = 2$	12,000	99	170	This work
Cu/(Cu + Ce) = 0.15 120 mg net catalysts on 300 mg Al foam	1% CO 1.25% O_2 50% H_2, and He balance, $\lambda = 2.5$	4,718	99	130–190	[45]
4% Pt–0.5% Fe/mordenite net mass of Pt–Fe catalysts: 216 mg	1% CO 1% O_2 and H_2 balance, $\lambda = 2$	9,500	>99	100–130	[46]
1% Pt/3A zeolite–Al_2O_3 net mass of Pt catalysts: 75 mg	37% H_2 5% H_2O 18% CO_2 0.5–1% CO 1–2% O_2, $\lambda = 4$	4,800	99.9	215-225	[47]

means smaller volume of catalysts at a constant gas flow rate. Therefore, preparing catalysts to meso-macroporous monolith can reduce the catalyst volume effectively.

For micro-channel reactors, metal foams, and general monoliths, the channel sizes are in hundreds of microns or about 1 mm. As H_2-rich gases pass through these channels at very high space velocity, part of CO in the gases will pass through without contacting with the surface of the catalysts. Therefore, CO can hardly be purified to ppm level. On this point, Chin and co-workers have suggested the existence of mass transfer resistance between the bulk gas and the catalyst surface [35, 36]. In the case of the macroporous monoliths, the macropores sized in the scale of several tens of microns, which are much smaller than those of the channels of the micro-channel reactors, metal foams, and general monoliths. Therefore, the mass transfer between the bulk gas and the catalyst surface can be improved markedly.

As stated above, the meso-macroporous monolithic catalysts can be made to any wanted shape, such as, chip like. CO can be removed as hydrogen-rich gases pass through the chip. In the case of the cylindrical monoliths of this work, the pressure drop of the reactant gases flowing through the channels of the monoliths is about 8 kPa at the gas volume velocity of 40 ml min^{-1}. Such small pressure drop is owing to the uniformity of the macropores in the monoliths, which is a key influencing factor for the pressure drop. The pressure drop can be reduced further, even close to zero, when the monoliths are shaped into thin chips. The size and structure of the meso–macropores can be tailored and controlled by changing preparation conditions. Therefore, this kind of catalytic materials is flexible in the application view. It is possible to be extended to other chemical reactions.

Conclusions

Meso-macroporous γ-Al_2O_3 monoliths with high surface areas can be made by using concentrated emulsion synthesis route. CuO–CeO_2 catalysts can be coated evenly onto the walls of the macropores of the γ-Al_2O_3 monolith with ceria and copper oxide highly dispersed. The coated CuO is present in three states, the first is the dispersed on ceria oxide, the second is on γ-alumina surface with parts of copper oxide particles' fringe in contact to ceria, and the third is on γ-alumina surface with no interaction to ceria. The former two kinds of CuO should be highly active for CO oxidation.

The prepared meso-macroporous monolithic CuO–CeO_2/γ-Al_2O_3 catalysts can remove CO from H_2-rich gases to ppm level at high space velocity, suggesting that making meso-macroporous monolithic catalysts is expected to be an effective way for the miniaturization of CO purification process and likely be extended to the miniaturization of other chemical reactions.

Acknowledgements The financial support of this work by Hi-tech Research and Development Program of China (863 program, Granted as No. 2007AA05Z104), National Natural Science foundation of China (No. 20976121) and the Cheung Kong Scholar Program for Innovative Teams of the Ministry of Education (No. IRT0641) are gratefully acknowledged.

References

1. Zhang Y, Zhao C, Liang H, Liu Y (2009) Catal Lett 127:339
2. Tseng HH, Kumar IA, Weng T-H, Lu C-Y, Wey M-Y (2009) Desalination 240:40
3. Gorte RJ, Vohs JM (2003) J Catal 216:477
4. Wang DW, Li F, Lu GQ, Cheng H-M (2008) Carbon 46:1593
5. Babin J, Iapichella J, Lefevre B, Biolley C, Bellat JP, Fajula F, Galarneau A (2007) New J Chem 31:1907
6. Ma TY, Zhang XJ, Yuan ZY (2009) Micropor Mesopor Mater 123:234
7. Zhong H, Liu J, Wang P, Yang J, Yang Q (2009) Micropor Mesopor Mater 123:63
8. Zhao Y, Zhang X, Zhai J, Jiang L, Liu Z, Nishimoto S, Murakami T, Fujishima A, Zhu D (2008) Micropor Mesopor Mater 116:710
9. Tidahy HL, Hosseni M, Siffert S, Cousin R, Lamonier JF, Aboukaïs A, Su BL, Giraudon JM, Leclercq G (2008) Catal Today 137:335
10. Idakiev V, Tabakova T, Tenchev K, Yuan Z, Ren T, Vantomme A, Su B (2009) J Mater Sci 44:6637. doi:10.1007/s10853-009-3574-9

11. Gennequin C, Lamallem M, Cousin R, Siffert S, Idakiev V, Tabakova T, Aboukaïs A, Su B (2009) J Mater Sci 44:6654. doi: 10.1007/s10853-009-3631-4
12. Reddy B, Reddy G, Ganesh I, Ferreira J (2009) J Mater Sci 44:2743. doi:10.1007/s10853-009-3358-2
13. Shao GS, Zhang XJ, Yuan ZY (2008) Appl Catal B Environ 82:208
14. Nowak I, Kilos B, Ziolek M, Lewandowska A (2003) Catal Today 78:487
15. Chiu JJ, Pine DJ, Bishop ST, Chmelka BF (2004) J Catal 221:400
16. Konishi J, Fujita K, Oiwa S, Nakanishi K, Hirao K (2008) Chem Mater 20:2165
17. Shi ZG, Feng YQ, Xu L, Zhang M, Da SL (2004) Talanta 63:593
18. Steinke JHG, Dunkin IR, Sherrington DC (1996) Macromolecules 29:5826
19. Lu AH, Smån t JH, Backlund S, Lindén M (2004) Micropor Mesopor Mater 72:59
20. Frenette G, Forthoffer D (2009) Int J Hydrogen Energy 34:3578
21. Whittingham MS, Savinell RF, Zawodzinski T (2004) Chem Rev 104:4243
22. Haryanto A, Fernando S, Murali N, Adhikari S (2005) Energy Fuel 19:2098
23. Godinho M, de F. Gonçalves R, Leite E, Raubach C, Carreño N, Probst L, Longo E, Fajardo H (2010) J Mater Sci 45:593. doi: 10.1007/s10853-009-3932-7
24. Igarashi H, Fujino T, Watanabe M (1995) J Electroanal Chem 391:119
25. Liu X, Wang A, Yang X, Zhang T, Mou C-Y, Su D-S, Li J (2008) Chem Mater 21:410
26. Naknam P, Luengnaruemitchai A, Wongkasemjit S, Osuwan S (2007) J Power Sources 165:353
27. Liu Y, Fu Q, Stephanopoulos MF (2004) Catal Today 93–95:241
28. Cao JL, Deng QF, Yuan ZY (2009) J Mater Sci 44:6663. doi: 10.1007/s10853-009-3582-9
29. Cao JL, Shao G-S, Ma T-Y, Wang Y, Ren T-Z, Wu S-H, Yuan Z-Y (2009) J Mater Sci 44:6717. doi:10.1007/s10853-009-3583-8
30. Guo Q, Liu Y (2008) Appl Catal B Environ 82:19
31. Salker AV, Gurav SM (2000) J Mater Sci 35:4713. doi: 10.1023/A:1004803123577
32. Zeng S, Liu Y, Wang Y (2007) Catal Lett 117:119–125
33. Williams JL (2001) Catal Today 69:3
34. Kim KY, Han J, Nam SW, Lim T-H, Lee H-I (2008) Catal Today 131:431
35. Chin P, Sun X, Roberts GW, Spivey JJ (2006) Appl Catal A Gen 302:22
36. Roberts GW, Chin P, Sun X, Spivey JJ (2003) Appl Catal B Environ 46:601
37. Zhang Y, Liang H, Zhao CY, Liu Y (2009) J Mater Sci 44:931. doi:10.1007/s10853-008-3189-6
38. Salasc S, Perrichon V, Primet M, Chevrier M, Mouaddib-Moral N (2000) J Catal 189:401
39. Jiang X, Lou L, Chen Y, Zheng X (2003) J Mol Catal A Chem 197:193
40. Pintar A, Batista J, Hocevar S (2005) J Colloid Interface Sci 285:218
41. Wan H, Li D, Dai Y, Hu Y, Zhang Y, Liu L, Zhao B, Liu B, Sun K, Dong L, Chen Y (2009) Appl Catal A Gen 360:26
42. Zhang SM, Huang WP, Qiu XH, Li BQ, Zheng XC, Wu SH (2002) Catal Lett 80:41
43. Liu W, Flytzani-Stephanopoulos M (1996) Chem Eng J Biochem Eng J 64:283
44. Gamarra D, Belver C, Fernandez-Garcia M, Martinez-Arias A (2007) J Am Chem Soc 129:12064
45. Papavasiliou J, Avgouropoulos G, Ioannides T (2006) Appl Catal B Environ 66:168
46. Maeda N, Matsushima T, Uchida H, Yamashita H, Watanabe M (2008) Appl Catal A Gen 341:93
47. Galletti C, Specchia S, Saracco G, Specchia V (2009) Chem Eng J 154:246